Applied Catalysis B: Environmental 162 (2015) 602–609

Contents lists available at ScienceDirect

Applied Catalysis B: Environmental

journal homepage: www.elsevier.com/locate/apcatb

Impact of feed impurities on catalysts for chlorine recycling

Maximilian Moser, Amol P. Amrute, Javier Pérez-Ramírez *

Institute for Chemical and Bioengineering, Department of Chemistry and Applied Biosciences, ETH Zurich, Vladimir-Prelog-Weg 1, CH-8093 Zurich, Switzerland

ARTICLE INFO

Article history:
Received 27 May 2014
Received in revised form 11 July 2014
Accepted 15 July 2014
Available online 22 July 2014

Keywords:
HCl oxidation
Deacon catalysts
Carbon monoxide
Sulfur compounds
Regeneration

ABSTRACT

This study assesses the impact of feed impurities on the design of a robust catalytic process for chlorine recycling *via* HCl oxidation (Deacon reaction). The influence of CO, SO_2, and COS was investigated over stable catalysts, including RuO_2/SnO_2-Al_2O_3, CeO_2/ZrO_2, U_3O_8/ZrO_2, IrO_2/TiO_2, and $CuCrO_2$. Carbon monoxide is detrimental for RuO_2- and IrO_2-based catalysts, since the highly exothermic oxidation to CO_2 under Deacon conditions causes pronounced temperature rises leading to material and reactor instabilities. Advantageously, the other catalysts are practically unaffected by this impurity due to their inactivity for CO oxidation in the chlorinated state. Carbonyl sulfide and particularly sulfur dioxide severely poison all the catalysts investigated due to the strong adsorption of the sulfur compounds and active site blockage. However, the initial activity can be restored by treating the deactivated catalysts in HCl (without oxygen) at the reaction temperature. We discuss process strategies for feed purification and catalyst regeneration depending on the chosen catalytic system, which are of utmost important for the ultimate sustainability of the process.

1. Introduction

The assessment of catalytic performance in academic studies is generally conducted under ideal conditions, that is, using model mixtures of the pure reactant(s). However, it is well known that feed streams in industry often contain a wide spectrum of impurities, which can detrimentally affect the catalytic performance [1,2]. For example, in the petroleum industry, hydrogenation processes, and catalytic converters, sulfur, nitrogen, halogens, and metals are prominent contaminants, inhibiting and/or poisoning catalysts [2–7]. Usually, these compounds have to be removed prior to the catalytic step by cost-intensive purification processes. Alternatively, the search for catalysts that tolerate impurities is highly attractive. An illustrative example of how critical feed impurities are for catalyst and process design comprises iron-loaded zeolites for N_2O abatement. Compared to other metals, iron exhibits moderate-to-low activity for N_2O decomposition in a standard feed containing only nitrous oxide [8]. However, compounds such as NO, CO, and SO_2 present in industrial tail gases boost the N_2O decomposition activity over Fe-zeolites, a crucial result for its today's wide industrial implementation [9].

In the last decade, the gas-phase oxidation of HCl to Cl_2 (Eq. (1)) has received considerable attention as a sustainable process to recycle the growing excess of byproduct HCl generated in the phosgene-mediated manufacture of polyurethanes and polycarbonates, due to its superior energy efficiency and environmental friendliness over alternative strategies such as HCl electrolysis or neutralization [10]. Intense research efforts led to the development of active catalysts based on RuO_2, CeO_2, U_3O_8, IrO_2, and $CuCrO_2$, which satisfy the stability requirements that rendered the original Deacon catalyst based on $CuCl_2$ and many other analogues impractical [11–15]. However, the performance of these catalytic systems may be affected by various contaminants that are present in industrial HCl-containing streams, such as CO, COS, SO_2, and H_2S (Scheme 1a) [16,17]. The patent literature discloses that CO can deactivate RuO_2-based catalysts for HCl oxidation at high temperatures, due to the formation of volatile metal carbonyls and/or carbonates [16]. Besides, the ability of the catalysts to oxidize CO to CO_2 under HCl oxidation conditions is critical, since the reaction is highly exothermic (Eq. (2)) and thus can lead to uncontrolled local temperature rises in the catalyst bed [16]. The resulting hot spots induce undesired sintering of the active RuO_2 phase and over-oxidation to the volatile RuO_4 [10]. With respect to sulfur compounds, it is known that RuO_2-based materials are thiophilic, leading to the formation of stable bonds with sulfur and thereby poisoning the active sites for HCl oxidation. Specifically, the presence of COS (11 ppm) and SO_2 (53 ppm) in the Deacon mixture

* Corresponding author. Fax: +41 44 633 1405.
E-mail address: jpr@chem.ethz.ch (J. Pérez-Ramírez).

http://dx.doi.org/10.1016/j.apcatb.2014.07.037
0926-3373/

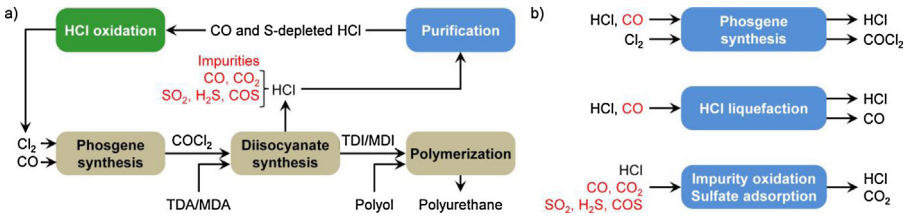

Scheme 1. (a) In the production of TDI (toluene diisocyanate) and MDI (methylene diphenyl diisocyanate), the HCl byproduct can be recycled to Cl_2 *via* catalyzed oxidation. The gaseous HCl stream, containing carbon monoxide and sulfur compounds, requires purification in order to prolong the catalyst lifetime. The different strategies to remove these impurities are depicted in (b).

($HCl + O_2$) reduced the activity of RuO_2/SnO_2-Al_2O_3 by 20 and 32% within the first 10 h on stream, respectively [17].

$$2HCl + 1/2O_2 \leftrightarrow Cl_2 + H_2O, \quad \Delta H_r^\circ = -56.8\,kJ\,mol^{-1} \tag{1}$$

$$CO + 1/2O_2 \rightarrow CO_2, \quad \Delta H_r^\circ = -283\,kJ\,mol^{-1} \tag{2}$$

As a consequence, the HCl stream has to be duly purified to ensure catalyst and process stability. Carbon monoxide can be removed by reaction with Cl_2 over activated carbon to form phosgene, which can be subsequently separated from HCl and fed to the diisocyanate synthesis (Scheme 1b, top) [16]. Alternatively, HCl can be liquefied by compression at elevated pressure, followed by the removal of the CO gas from the HCl liquid and the evaporation of the latter in the Deacon reactor (Scheme 1b, middle) [18]. More conveniently, the catalyzed CO oxidation to CO_2 can be conducted over a conventional noble metal-based catalyst prior to the HCl oxidation reactor (Scheme 1b, bottom) [19,20]. The latter approach also removes sulfur compounds by their oxidation and subsequent adsorption of the resulting sulfate on the same catalyst.

With the exception of some patents dealing with RuO_2-based catalysts, the role of impurities in HCl-containing streams on other relevant Deacon catalysts (possessing very different intrinsic properties and operating temperatures) remains unexplored. We herein assess the individual and combined impact of CO, SO_2, and COS on the HCl oxidation performance of RuO_2/SnO_2-Al_2O_3, IrO_2/TiO_2, CeO_2/ZrO_2, U_3O_8/ZrO_2, and $CuCrO_2$. The activity and stability patterns of these catalytic materials in relation to these contaminants are quantified by means of temperature-programmed and steady-state tests. This understanding is necessary to evaluate the sensitivity of promising catalysts to technical process conditions, which ultimately determines the extent of the feed purification and the design of suitable regeneration strategies.

2. Experimental

2.1. Catalysts

The preparation and characterization of the catalysts used in this study have been detailed in recent publications [11–15]. Briefly, RuO_2/SnO_2-Al_2O_3 (2 wt.% Ru, $S_{BET} = 29\,m^2\,g^{-1}$), IrO_2/TiO_2 (2 wt.% Ir, $S_{BET} = 24\,m^2\,g^{-1}$), CeO_2/ZrO_2 (7.7 wt.% Ce, $S_{BET} = 48\,m^2\,g^{-1}$), and U_3O_8/ZrO_2 (9.8 wt.% U, $S_{BET} = 35\,m^2\,g^{-1}$), were prepared by incipient wetness impregnation of corresponding carriers with aqueous solutions of $RuCl_3 \cdot xH_2O$, $IrCl_3 \cdot xH_2O$, $Ce(NO_3)_3 \cdot 6H_2O$, and $UO_2(NO_3)_2 \cdot 6H_2O$, respectively, followed by drying and calcination. Bulk $CuCrO_2$ ($1\,m^2\,g^{-1}$) was synthesized by static-air calcination of a ball-milled equimolar mixture of Cu_2O and Cr_2O_3 at 1373 K for 30 h.

2.2. Methods

The metal content in the fresh and used catalysts was determined by X-ray fluorescence (XRF) using an Orbis Micro-EDXRF with a Rh source (50 kV) and a silicon drift detector. The amounts of carbon and sulfur were measured by quantitative infrared spectroscopy performed using a LECO CHN-900 combustion furnace. Powder X-ray diffraction (XRD) patterns were acquired in a PANalytical X'Pert PRO-MPD diffractometer. Data were recorded in the 10–70° 2θ range with an angular step size of 0.017° and a counting time of 0.26 s per step. N_2 sorption at 77 K was measured in a Quantachrome Quadrasorb-SI analyzer. Prior to the measurement, the samples were evacuated at 473 K for 12 h. Diffuse reflectance infrared Fourier transform spectroscopy (DRIFTS) was performed at 473 K under N_2 atmosphere using a Bruker Vertex 70 spectrometer. Prior to the measurement, the samples were dried at 573 K in N_2 ($100\,cm^3\,STP\,min^{-1}$) for 1 h. Spectra were recorded in the range of 700–1500 cm^{-1} with a nominal resolution of $4\,cm^{-1}$ and co-addition of 200 scans.

2.3. Catalytic tests

Catalytic tests were performed in a home-made continuous-flow micro-reactor. The catalyst (0.25 g, particle size = 0.4–0.6 mm) was loaded in a quartz tube (8 mm i.d.) between two plugs of quartz wool. Temperature-programmed reactions (TPR) and steady-state experiments were performed at ambient pressure using feed mixtures containing 10 vol.% HCl, 20 vol.% O_2, with or without addition of 1 vol.% CO, 0.03 vol.% COS, 0.03 vol.% SO_2, and 2 vol.% Ar, balanced in He, at a total volumetric flow of $166\,cm^3\,STP\,min^{-1}$. TPR experiments in $HCl + O_2$, $CO + O_2$, and $HCl + CO + O_2$ were carried out by ramping the furnace temperature in the range of 353–773 K at $5\,K\,min^{-1}$ to derive the light-off temperatures of the catalysts for Cl_2 and CO_2 production. Steady-state tests were performed at temperatures of 603 K (RuO_2/SnO_2-Al_2O_3), 703 K (CeO_2/ZrO_2), and 723 K (IrO_2/TiO_2), to quantitatively determine deactivation behaviors in different feed mixtures as well as to measure the bed temperature rise caused by the presence of carbon monoxide. The apparent activation energies for HCl and CO oxidation were measured between 543 and 660 K under steady-state conditions in a mixture of $HCl + CO + O_2$. Kinetic experiments of CO oxidation over RuO_2/SnO_2-Al_2O_3 were conducted at variable inlet CO concentration (0.5–3 vol.%) and 20 vol.% O_2 at 603 K. The sulfur-poisoned catalysts were regenerated in a feed containing 10 vol.% HCl in He at the reaction temperature of the corresponding system. Selected samples were collected after the catalytic tests for characterization by rapidly cooling down the reactor to room temperature in a He flow.

Online analysis was carried out using an OmniStar mass spectrometer (MS) from Pfeiffer Vacuum equipped with an yttria-coated iridium cathode and connected to the reactor outlet with a quartz capillary (length = 1.5 m, i.d. = 0.75 μm) heated at 413 K. The ion currents of AMU (atomic mass units) 28 (CO), 44 (CO_2), 64 (SO_2), and 70 (Cl_2) were normalized to the internal standard (Ar, AMU 40). The CO signal was calibrated prior to the experiments in order to quantify the CO conversion. The percentage of CO conversion was determined as $X_{CO} = [(\text{mol CO}_{inlet} - \text{mol CO}_{outlet})/\text{mol CO}_{inlet}] \times 100$. The amount of

Cl_2 was quantified by means of iodometric titration using a Mettler Toledo G20 Compact Titrator. The percentage of HCl conversion was determined as $X_{HCl} = [2 \times \text{mol } Cl_{2,outlet}/\text{mol } HCl_{inlet}] \times 100$.

3. Reactor modeling

Reactor simulations were undertaken to assess the impact of CO oxidation on the operation of an adiabatic reactor for HCl oxidation over RuO_2/SnO_2-Al_2O_3. The reactor model was adapted from recent work on HBr oxidation to Br_2 [21], using the design and operation parameters of a pilot-plant unit [22]. The apparent kinetic parameters of the catalyst were obtained from the linear fit of the data points in the Arrhenius plot and implemented in Eq. (3):

$$k(T) = k_0^{app} \exp\left(-\frac{E_a^{app}}{RT}\right) \quad (3)$$

where k (mol h^{-1} kg_{cat}^{-1} bar^n) is the reaction rate constant, k_0^{app} (mol h^{-1} kg_{cat}^{-1} bar^n) is the apparent pre-exponential factor, E_a^{app} (kJ mol^{-1}) is the apparent activation energy, T (K) is the temperature, and R (8.3145 J mol^{-1} K^{-1}) is the universal gas constant. The specific reaction rate r_i (mol_i h^{-1} kg_{cat}^{-1}) for HCl oxidation (Eq. (4)) and CO oxidation (Eq. (5)) were modeled by implementing a power law rate expression:

$$r_{Cl_2}(T) = k_{Cl_2}(T) y_{HCl} y_{O_2}^{0.5} P^{1.5} - \frac{k_{Cl_2}(T)}{K_{eq}(T)} y_{Cl_2} y_{H_2O} P^2 \quad (4)$$

$$r_{CO_2}(T) = k_{CO_2}(T) y_{CO}^{-0.4} P^{-0.4} \quad (5)$$

where K_{eq} ($bar^{0.5}$) is the equilibrium constant for HCl oxidation, y_i (–) is the molar fraction of component i, and P (bar) is the total pressure. The model assumed ideal gas behavior, steady-state conditions, a plug-flow velocity profile, and a negligible pressure drop. Furthermore, possible transport gradients in the catalyst bed or single catalyst particles were not accounted for [21]. The reactor design equations for all components ($i = O_2$, H_2O, HCl, Cl_2, CO, CO_2) can be written as:

$$\frac{dF_i}{dW_{cat}} = \frac{\nu_i}{\nu_{Cl_2}} r_{Cl_2}(T) \quad (6)$$

$$\frac{dF_i}{dW_{cat}} = \frac{\nu_i}{\nu_{CO_2}} r_{CO_2}(T) \quad (7)$$

where F_i (mol STP h^{-1}) is the molar flow rate of component i, W_{cat} (kg) is the catalyst weight, and ν_i is the stoichiometric coefficient of component i. The energy balance for the adiabatic reactor can be defined as:

$$\frac{dT}{dW_{cat}} = \frac{-\Delta H_{r,CO} r_{CO_2}(T) - \Delta H_{r,Cl_2} r_{Cl_2}(T)}{\sum_N^{i=1} F_i c_{p,i}} \quad (8)$$

where ΔH_r (kJ mol^{-1}) is the reaction enthalpy and $c_{p,i}$ (J mol^{-1} K^{-1}) is the specific heat capacity of component i. Based on this model, we simulated the conversion of HCl an CO in an adiabatic reactor filled with 2 kg of catalyst using a feed mixture containing 10 vol.% HCl, 30 vol.% O_2, and 0–1 vol.% CO (balanced in N_2), an inlet volumetric flow of 30 m^3 STP h^{-1}, and a total pressure of 3.4 bar.

4. Results and discussion

4.1. Influence of carbon monoxide

The CO impurity results from the phosgene synthesis step prior to the diisocyanate synthesis and can reach up to 10 vol.% in the technical HCl stream [17,19]. Our investigation was conducted using 1 vol% CO in the total flow in order to simulate the industrial conditions. Temperature-programmed reactions coupled to online MS analysis in $HCl + O_2$, $CO + O_2$, and $HCl + CO + O_2$ mixtures were carried out to assess the influence of CO (HCl) on the activity of the catalysts for HCl (CO) oxidation (Fig. 1). The suitability of this transient method has been previously demonstrated for HCl oxidation over RuO_2- and Cu-based catalysts using online UV/vis analysis [23]. The light-off temperatures for Cl_2 production in $HCl + O_2$ (Fig. 1, top, dotted lines) reveals the following activity order: RuO_2/SnO_2-Al_2O_3 > >IrO_2/TiO_2 > $CuCrO_2$ ~ CeO_2/ZrO_2 > U_3O_8/ZrO_2, which is in agreement with the results of steady-state experiments published elsewhere [11–15]. The Cl_2 profiles in $HCl + CO + O_2$ and $HCl + O_2$ were practically identical over the catalysts (Fig. 1, top). The invariable HCl oxidation activity in the presence of CO is a key result, inferring that carbon monoxide does not block active sites for chlorine production. The only exception was IrO_2/TiO_2, which experienced a shift in the light-off temperature for Cl_2 evolution by 70 K in the presence of CO and suggests competitive adsorption of HCl and CO on the active coordinatively unsaturated iridium sites of the IrO_2 surface. This result is further substantiated by DFT calculations, indicating that the adsorption of CO (2.2 eV) is stronger on IrO_2(1 1 0) surface than that of HCl (1.5 eV) [14,24]. Differently, on RuO_2(1 1 0), the adsorption energy of HCl (1.4 eV) is slightly larger than that of CO (1.2 eV) [14,25]. All of the catalysts evaluated were active for the oxidation of CO in $CO + O_2$ and display much lower light-off temperatures than for the oxidation of HCl in $HCl + O_2$ (Fig. 1, bottom, dashed lines). The order of CO oxidation activity is RuO_2/SnO_2-Al_2O_3 ~ IrO_2/TiO_2 ~ $CuCrO_2$ > CeO_2/ZrO_2 > U_3O_8/ZrO_2. However, the oxidation of CO is strongly inhibited in the presence of HCl. The light-off temperature for CO_2 evolution over RuO_2/SnO_2-Al_2O_3 and IrO_2/TiO_2 in $HCl + CO + O_2$ is shifted by *ca.* 70 K compared to $CO + O_2$ and the production of CO_2 in the presence of HCl is suppressed over CeO_2/ZrO_2, U_3O_8/ZrO_2, and $CuCrO_2$. This result indicates that the oxidation of CO is inhibited and even extinguished over chlorinated surfaces, which agrees with the poisoning effect of chlorine reported over Au/TiO_2 and ceria-zirconia mixed oxides for CO and VOC oxidation, respectively [26,27]. RuO_2/SnO_2-Al_2O_3 and IrO_2/TiO_2 catalyze the highly exothermic CO oxidation at Cl_2 evolution temperatures (Fig. 1a and b, inset in top panel), which is disadvantageous for the technical application of the catalytic HCl oxidation process due to the additional heat generated (vide infra). Both comprise the most active Deacon catalysts, that is, they have a low energy demand for atomic chlorine recombination to the gas-phase Cl_2 [14]. Hence, at the Cl_2 evolution temperature, CO can be oxidized to CO_2 (Fig. 1a, top inset) over the free active sites on the partially chlorinated surface, as exemplified for RuO_2 (Fig. 1a, inset in bottom panel). It is plausible that the degree of surface chlorination over CeO_2/ZrO_2, U_3O_8/ZrO_2, and $CuCrO_2$ is more pronounced, thereby preventing the adsorption of CO on catalytically active centers within the observed temperature range (Fig. 1c–e, top inset). In view of these results, it is likely that a higher degree of surface chlorination could suppress the oxidation of CO on RuO_2/SnO_2-Al_2O_3, which reduces the risk of hot spots and catalyst deactivation by volatilization and/or sintering. Therefore, TPR experiments on RuO_2/SnO_2-Al_2O_3 were performed in a mixture of $HCl + CO + O_2$ applying a lower oxygen content (Fig. S1). The light-off temperatures for CO and HCl oxidation are similarly shifted to higher temperatures. The shift of the Cl_2 production is related to the increased degree of surface chlorination as previously demonstrated [28]. However, the oxidation of CO was not suppressed, thus a technical process using RuO_2-based catalysts could still suffer from the additional heat generated by the CO conversion (Section 4.2).

Steady-state experiments at fixed furnace temperatures in $HCl + O_2$ and $HCl + CO + O_2$ were conducted to quantify the temperature rise due to the simultaneous CO and HCl oxidation and to investigate the effect of CO on the steady-state HCl oxidation

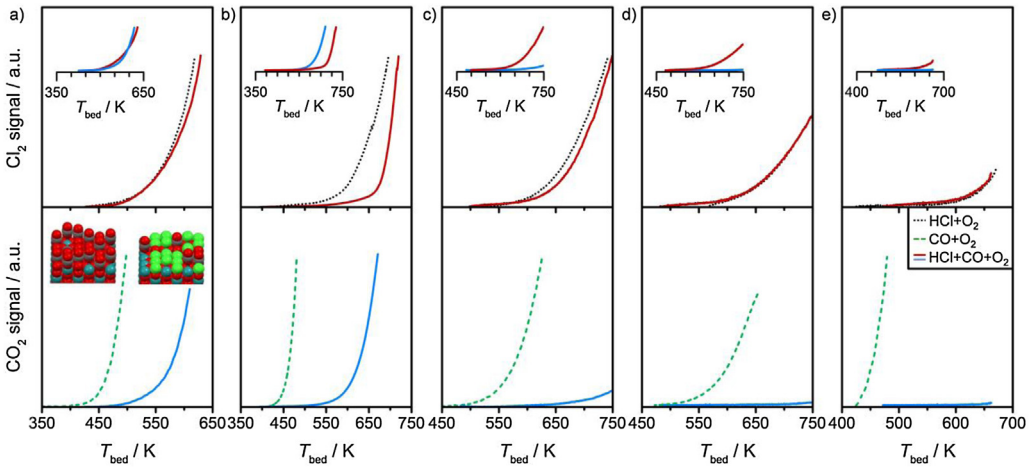

Fig. 1. Cl_2 and CO_2 signals *versus* bed temperature during TPR tests in HCl + O_2 (HCl:O_2 = 10:20, dotted line), CO + O_2 (CO:O_2 = 1:20, dashed line), and HCl + CO + O_2 (HCl:CO:O_2 = 10:1:20, solid lines) over (a) RuO_2/SnO_2-Al_2O_3, (b) IrO_2/TiO_2, (c) CeO_2/ZrO_2, (d) U_3O_8/ZrO_2, and (e) $CuCrO_2$. The insets in the top graphs compare the light-off curves of the catalysts for HCl oxidation (red line) and CO oxidation (blue line) in HCl + CO + O_2. The inset in the bottom of graph (a) illustrates the CO coverage on the oxidized (left) and chlorinated surface (right) of RuO_2. The adsorption of CO on chlorinated surfaces is hampered, which leads to the shift of the CO_2 evolution to higher temperatures (a–c) or even to the suppression of CO oxidation (d, e).

activity (Fig. 2). These tests were carried out over RuO_2/SnO_2-Al_2O_3 (603 K), IrO_2/TiO_2 (723 K), and CeO_2/ZrO_2 (703 K). U_3O_8/ZrO_2 and $CuCrO_2$ were not assessed due to their comparable behavior to CeO_2/ZrO_2 in the temperature-programmed tests (Fig. 1). The introduction of the HCl + O_2 feed to the reactor led to an increase in the bed temperature over all of the three catalysts (Fig. 2) by *ca.* 4 K due to the mild exothermic nature of HCl oxidation. The conversion levels of HCl (X_{HCl} = 24%, 30%, and 22%) and the bed temperature (T_{bed} = 607 K, 727 K, and 707 K) remained stable during 2 h on stream over RuO_2, IrO_2, and CeO_2-based samples, respectively. A further increase of the bed temperature over RuO_2/SnO_2-Al_2O_3 and IrO_2/TiO_2 was observed upon adding CO to the HCl + O_2 feed caused by the high exothermicity of the CO oxidation. The RuO_2-based system showed a lower exothermic temperature rise (15 K) than the IrO_2-based catalyst (25 K), which corresponds to the difference in the CO conversion levels of 60 and 85%, respectively.

RuO_2/SnO_2-Al_2O_3 exhibited a higher HCl conversion in HCl + CO + O_2 (X_{HCl} = 30%) than in HCl + O_2, which is not a result of CO promotion but mainly caused by the higher temperature rise compared to the HCl oxidation in HCl + O_2. This is corroborated by an additional experiment confirming that the HCl conversion is similar in both HCl + O_2 and HCl + CO + O_2 feed mixtures at the same bed temperature Fig. 2b). No such increase in the HCl conversion on IrO_2/TiO_2 was observed despite the temperature rise of 25 K (*i.e.* T_{bed} = 748 K) in HCl + CO + O_2 (Fig. 2c). However, a comparison at the same elevated bed temperature (T_{bed} = 748 K) revealed that the HCl conversion is higher in HCl + O_2 ($X_{HCl} \sim 40\%$) than in HCl + CO + O_2 ($X_{HCl} \sim 30\%$) (Fig. 2c). This indicates that the CO coverage on IrO_2/TiO_2 in HCl + CO + O_2 must be high, leading to a high CO conversion and thus inhibiting the HCl oxidation. This observation coincides with the shift in the light off for Cl_2 production to higher temperatures in HCl + CO + O_2 (Fig. 1b). In contrast, CeO_2/ZrO_2 experienced an insignificant rise in the bed temperature upon addition of CO to the HCl + O_2 feed and the CO conversion was below 3% (Fig. 2d). Moreover, the HCl conversion was also unaltered in HCl + CO + O_2.

The long-term performance of the technically most relevant technical catalysts, RuO_2/SnO_2-Al_2O_3 and CeO_2/ZrO_2, was compared in HCl + CO + O_2 (Fig. 3a and b). The HCl conversion over the ceria catalyst remained unaffected in the presence of CO during 50 h on stream. The slight drop in HCl conversion over RuO_2/SnO_2-Al_2O_3 in the first 5 h (Fig. 3a) is likely due to the agglomeration of ruthenium species during the equilibration of the catalyst under the reaction environment [11]. The CO conversion over RuO_2/SnO_2-Al_2O_3 (X_{CO} = 60%) experienced activation during the first 5 h and steadily dropped during the next 45 h on stream. The latter could be related to the increase in the chlorine coverage with reaction time [28]. The CO conversion over CeO_2/ZrO_2 was negligible throughout the duration of the experiment (Fig. 3b). This result highlights the tolerance of the CeO_2-based system to CO impurities in technical HCl-containing streams.

The fresh and used catalysts were characterized to analyze the structural alterations due to the presence of CO. The X-ray diffractograms of the samples after the temperature-programmed tests (Fig. S2) and the long-term stability tests (Fig. S3) in HCl + CO + O_2 were identical to those of the corresponding as-prepared samples indicating no bulk modification . The compositional analysis was only performed for the samples of the long-term performance test, because they were exposed to CO for a significant amount of time. The Ru and Ce contents in the respective systems after 50 h steady-state test (2.3 and 7.7 wt.%, respectively) did not change with espect to their fresh analogues, indicating very slow or no volatilization of the active metals through potential carbonylation. The carbon content after testing in HCl + CO + O_2 on both RuO_2- and CeO_2-based samples was as low as 0.1 wt.%, which suggests that the CO impurity did not form any stable species on the catalysts surface and the catalyst did not suffer from any sort of coking.

4.2. *Impact of CO oxidation on Cl_2 production in an adiabatic reactor*

The simultaneous oxidation of CO and HCl in a HCl + CO + O_2 gas feed was simulated to exemplify the sensitivity of the temperature rise to different inlet CO concentrations (0–1 vol.%). The process was modeled on a RuO_2/SnO_2-Al_2O_3 catalyst in a single-stage adiabatic fixed-bed reactor. The kinetic parameters used in the simulation were determined experimentally over this catalyst in the laboratory. The pre-exponential factor was 1.5×10^7 mol Cl_2 h^{-1} kg_{cat}^{-1} $bar^{-1.5}$ and 2.3×10^9 mol CO_2 h^{-1} kg_{cat}^{-1} $bar^{0.4}$ for HCl and CO oxidations, respectively. The apparent activation energy for HCl oxidation was 68 kJ mol^{-1} and for CO oxidation it was 97 kJ mol^{-1}. The latter value for CO oxidation is higher in our case than that reported over the RuO_2-based catalyst [29], which is likely due to the simultaneous HCl oxidation under our reaction conditions. The CO

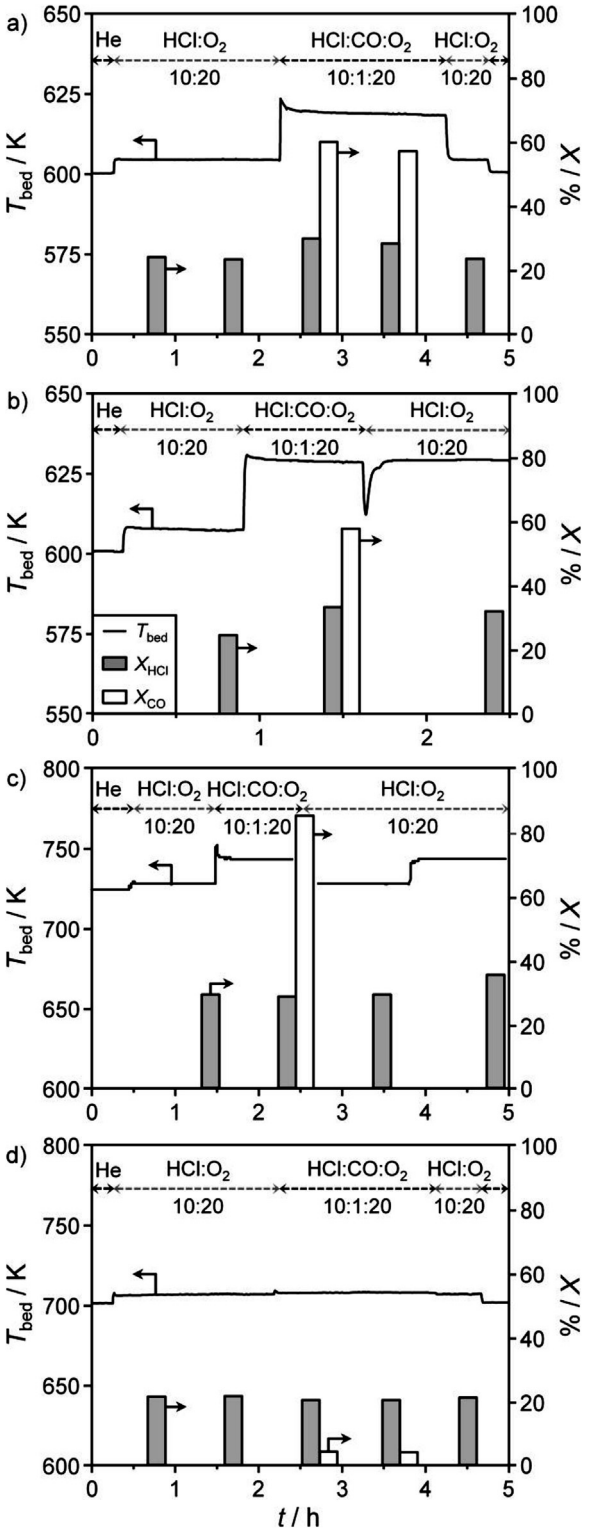

Fig. 2. Bed temperature (solid line) and conversion of HCl (grey bars) and CO (open bars) *versus* time-on-stream in steady-state tests over (a, b) RuO_2/SnO_2-Al_2O_3, (c) IrO_2/TiO_2, and (d) CeO_2/ZrO_2 using different feed compositions as specified in the figure. The steady-state test of RuO_2/SnO_2-Al_2O_3 is displayed in two separate graphs. In (a) the temperature rise due to the presence of CO in the feed is shown. In (b) the effect of CO addition on the HCl conversion under isothermal conditions is displayed.

partial pressure dependence was negative (−0.4) due to the low $CO:O_2$ ratio of 0.5–3:20 [30].

The simulations indicate that the temperature rise is very sensitive to the variation in CO concentration (Fig. 4a). The stepwise

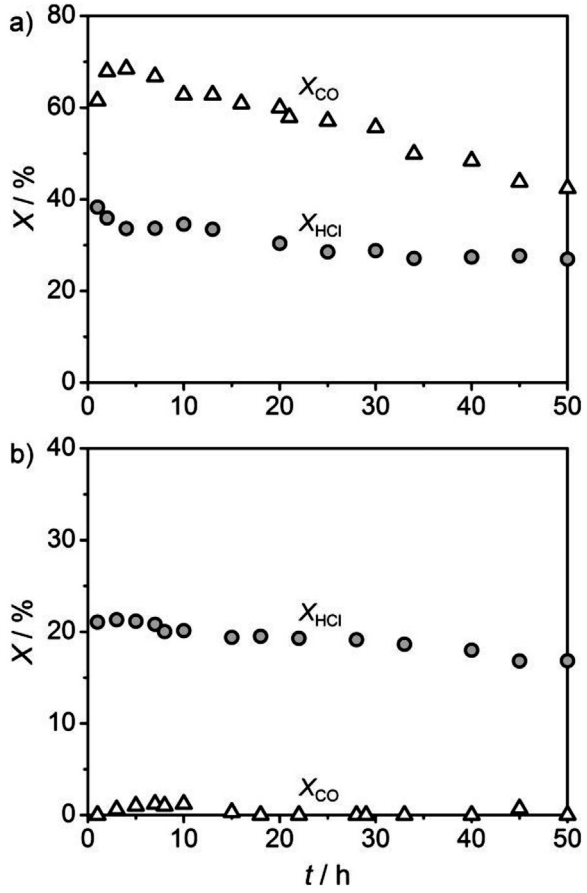

Fig. 3. Conversion of HCl and CO *versus* time-on-stream over (a) RuO_2/SnO_2-Al_2O_3 at 623 K and (b) CeO_2/ZrO_2 at 703 K in HCl + CO + O_2 (HCl:CO:O_2 = 10:1:20).

increase of the CO content from 0.1 to 1 vol.% led to steep temperature rises within the first 20% of the catalyst bed (Fig. 4a). This is obviously due to the exothermic nature and fast kinetics of the CO oxidation. The increased temperature also enhanced the HCl conversion (Fig. 4b), which is in line with the steady-state experiments over RuO_2/SnO_2-Al_2O_3 (Fig. 2a). However, owing to the likeliness of the formation of volatile RuO_4 and RuO_2 sintering, a RuO_2-based catalytic process has stringent limits regarding an upper limit in operating temperature [10]. Thus, in an adiabatic reactor, if the temperature rise due to CO oxidation is higher, the operating temperature limit (*i.e.* 673 K) will be reached faster and hence less HCl can be converted leading to the under-utilization of the catalyst bed (Fig. 4). Consequently, the CO content in the HCl stream must be constantly monitored and kept very low (<0.5 vol% CO [16]) to avoid a temperature overshoot and to improve the performance of the adiabatic HCl oxidation. These purification requirements of the HCl stream are costly. In this respect, CeO_2/ZrO_2 does not catalyze the CO oxidation in the presence of HCl and therefore offers clear advantages as it does not require the removal of CO prior to HCl oxidation.

4.3. Influence of sulfur compounds

Sources of sulfur compounds (SO_2/COS) in HCl stream, originating as byproduct of the diisocyanate production, include CO, Cl_2, toluene diamine (TDA), or methylene diphenyl diamine (MDA) (Scheme 1a). The concentration of the sulfur compounds in the HCl stream depends mostly on the quality of the CO and its own original source, *viz.* gas or coal. Furthermore, the efficiency of separation units and the quality of other feed components in diisocyanate

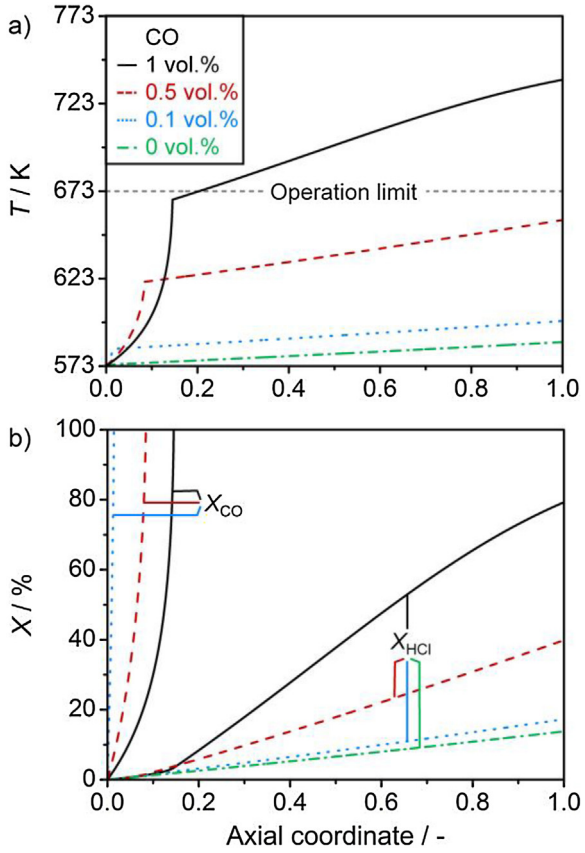

Fig. 4. Simulated temperature (a) and conversion (b) profiles in the axial direction of a fixed-bed reactor with RuO_2/SnO_2-Al_2O_3 in HCl:CO:O_2 mixtures at variable inlet CO concentration.

manufacture also influence the sulfur concentration in the HCl stream. The amount of sulfur compounds after purification should be in the range of 1-100 ppm, as specified in the patent literature [17]. Based on this range and the available experimental data disclosed in the patent application, we selected a sulfur concentration of 300 ppm to simulate a technical HCl stream. The impact of SO_2 on the performance of RuO_2/SnO_2-Al_2O_3 and CeO_2/ZrO_2 was investigated by temperature-programmed reactions. These experiments in HCl + SO_2 + O_2 feed clearly demonstrated a shift of the light-off curves for Cl_2 production to higher temperatures compared to HCl + O_2 for both the systems (Fig. 5), indicating a deactivation of both catalysts through SO_2 poisoning. The influence of SO_2 and COS is further addressed by steady-state tests to quantify the activity loss (Fig. 6). The HCl conversion in HCl + O_2

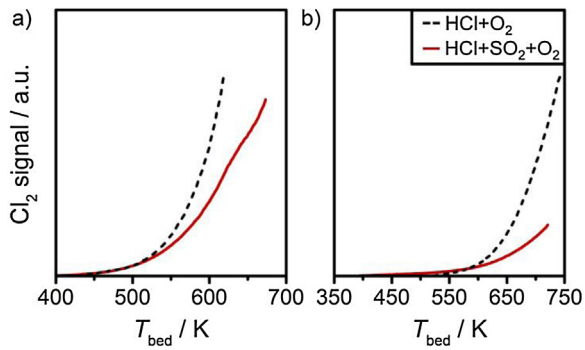

Fig. 5. Cl_2 signal *versus* bed temperature during TPR tests in HCl + O_2 (HCl:O_2 = 10:20, dashed line) and HCl + SO_2 + O_2 (HCl:SO_2:O_2 = 10:0.03:20, solid line) over (a) RuO_2/SnO_2-Al_2O_3 and (b) CeO_2/ZrO_2.

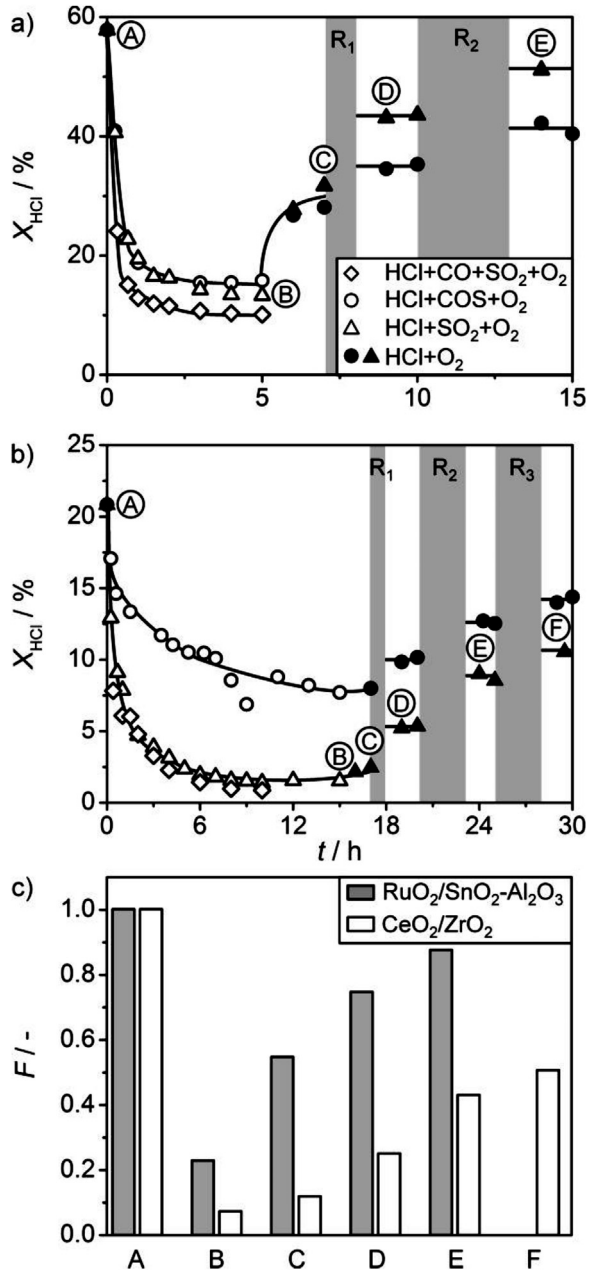

Fig. 6. HCl conversion *versus* time-on-stream over (a) RuO_2/SnO_2-Al_2O_3 at 623 K and (b) CeO_2/ZrO_2 at 703 K in the presence of sulfur compounds and carbon monoxide. Once the HCl conversion was stabilized, the impurities were removed restoring the standard HCl + O_2 mixture. The sulfur-poisoned catalysts were successfully regenerated in several intervals (R_1–R_3) by feeding a mixture of 10 vol.% HCl in helium at the reaction temperature of the corresponding catalyst. (c) Fraction of initial activity of RuO_2/SnO_2-Al_2O_3 (grey bars) and CeO_2/ZrO_2 (white bars) for selected points (A-F) during the poisoning and regeneration experiments.

amounted to 60% and 22% for RuO_2/SnO_2-Al_2O_3 and CeO_2/ZrO_2, respectively. Upon co-feeding of either COS or SO_2, the HCl conversion over RuO_2/SnO_2-Al_2O_3 dropped to 14% after 5 h on stream (Fig. 6a), which is *ca.* 23% of its initial activity (Fig. 6c, B). In the case of CeO_2/ZrO_2, the HCl conversion decreased to 2% and 8% for SO_2 and COS poisoning after 15 h, respectively (Fig. 6b). The slower deactivation of CeO_2/ZrO_2 compared to RuO_2/SnO_2-Al_2O_3 is likely caused by the higher surface chlorination of the former, hindering the adsorption of the sulfur compounds on its surface. Furthermore, SO_2 represents a significantly stronger poison for CeO_2/ZrO_2 compared to COS, leading to a decrease in the activity of CeO_2/ZrO_2 less

than 10% of its initial value (Fig. 6c, B). The more detrimental effect of SO_2 poisoning than that of COS on CeO_2-based catalysts suggests that the former species is more reactive and strongly bonded on the catalyst surface compared to the latter. The sulfur poisoning can be counterbalanced by the presence of CO through the reduction of surface sulfate species on the catalysts. This effect was observed at elevated temperatures (>750 K) for CeO_2 and ZrO_2 [31], however, under HCl oxidation conditions, the presence of CO in the feed (*i.e.* $HCl + CO + SO_2 + O_2$) did not significantly affect the deactivation trends on either RuO_2/SnO_2-Al_2O_3 and CeO_2/ZrO_2 (Fig. 6a and b).

After stabilization of the HCl conversion in the $HCl + SO_2/COS + O_2$ feed mixtures, the sulfur component was removed from the feed stream, and a $HCl + O_2$ stream was fed to the catalyst bed for the next 2 h (Fig. 6a and b). Under the latter conditions, RuO_2/SnO_2-Al_2O_3 regained half of its initial activity, while CeO_2/ZrO_2 did not show any significant reactivation (Fig. 6c, C). In order to enhance the activity recovery, both catalysts were regenerated in a diluted HCl stream, as it was proposed by Schmidt et al. for the regeneration of RuO_2-based catalysts following COS and SO_2 poisoning [32]. In the absence of oxygen, it is likely that HCl strongly chlorinates the surface and reduces the surface sulfur species, which then readily desorb from the catalyst surface. To monitor the efficiency of the regeneration, the activity was measured under model feed conditions ($HCl + O_2$) in between the regeneration cycles (Fig. 6c, D–F). In the case of SO_2 poisoning, RuO_2/SnO_2-Al_2O_3 regained up to 88% of its initial activity after a total of 4 h of regeneration (Fig. 6c, E), while CeO_2/ZrO_2 recovered just 55% even after a total of 7 h of regeneration (Fig. 6c, F). With regard to COS, both catalysts recovered *ca.* 70% of their initial activity (Fig. 6a and b). The slower regeneration of CeO_2/ZrO_2 compared to RuO_2/SnO_2-Al_2O_3 could result from a stronger adsorption of sulfur compounds.

Insights into the catalyst poisoning by sulfur were gained *via* characterization of the fresh and used catalysts. The ruthenium and cerium contents in the corresponding catalysts, with respect to their fresh analogues, remained unaltered upon testing in the sulfur-containing feeds and regeneration steps. The fresh RuO_2/SnO_2-Al_2O_3 and CeO_2/ZrO_2 samples exhibited very little amount of sulfur (*ca.* 0.01 wt.%). Upon poisoning in the $HCl + SO_2 + O_2$ feed, the sulfur content in these catalysts raised to 0.9 wt.% and 2 wt.%, respectively. After 4 h of regeneration in HCl, the sulfur content in RuO_2/SnO_2-Al_2O_3 dropped to 0.4 wt.% (*i.e.* by 55%), while for CeO_2/ZrO_2, it decreased to only 1.4 wt.% (*i.e.* by 30%) even after 7 h of regeneration (see F in Fig. 6). These results indicate that sulfur compounds are more strongly adsorbed on the CeO_2-based catalyst than on the RuO_2-based system. In fact, CeO_2/ZrO_2 has been reported to retain large amounts of sulfur and suggested to form bulk sulfates [31]. Bulk sulfate species were not observed by XRD analysis (Fig. S3). It could be plausible owing to low sulfur content that the poisoning is mostly located on the catalyst surface blocking the active sites. To identify the nature of the adsorbed sulfur species, the CeO_2-based samples were studied by infrared spectroscopy (Fig. 7). Upon poisoning with SO_2 and COS, a broad increase of the bands was observed between 1400 and 900 cm^{-1}. The signal between 1100 and 900 cm^{-1} could be assigned to adsorbed SO_3^{2-} or HSO_3^- species [31] and the large and broad signal between 1400 and 1100 cm^{-1} to the strongly adsorbed surface SO_4^{2-} species [33]. The signal intensity of the SO_2 poisoned samples was larger than that of COS poisoned samples (Fig. 7, inset), which is also in line with the sulfur content of 2 wt.% and 1 wt.%, respectively. This could be due to the direct oxidation of SO_2 to SO_3^- and SO_4^{2-} species that strongly adsorb on the surface [31], whereas for COS, it is possible that CeO_2 catalyzes the hydrolysis to $CO_2 + H_2S$ like it was reported for Al_2O_3 [34]. This could eventually lead to the different degree of deactivation

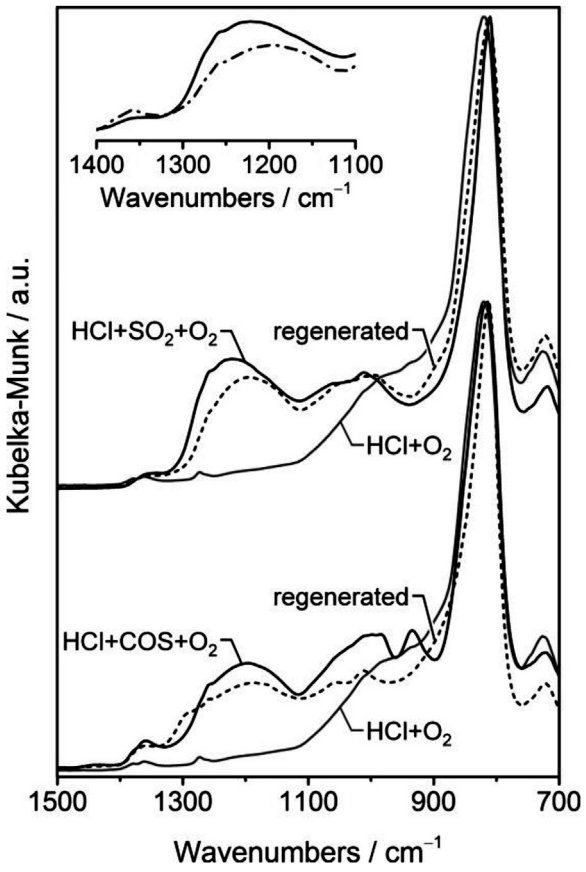

Fig. 7. Infrared spectra of CeO_2/ZrO_2 before and after addition of SO_2 and COS to the $HCl + O_2$ feed, and after regeneration in HCl. The inset plots the spectra after tests with SO_2 (solid line) and COS (dash-dotted line).

compared to SO_2 poisoning (Fig. 6b). After regeneration (Fig. 6b, F), both CeO_2-based catalysts exhibited a reduction of the infrared signals within the respected range of 1400–900 cm^{-1} (Fig. 7), which coincides with the lower sulfur content (vide supra). Interestingly, even with 70% of the sulfur still remaining at the surface of the CeO_2/ZrO_2 catalyst after regeneration, *ca.* 50% of the initial activity was recovered. In view of the sulfate species being more stable and difficult to remove from ZrO_2 than from CeO_2 [31], our results suggest that the HCl treatment regenerated the large fraction of the active sites in the ceria phase, while the significant amount of the remaining sulfur may remain accumulated on the zirconia carrier. The investigation of the RuO_2-based samples with infrared spectroscopy was attempted. However, no useful data could be obtained due to the strong absorption of the infrared light by the material.

4.4. Process implications

The severe impact of feed contaminants on the performance of the catalysts necessitates the installation of a guard bed to remove CO and sulfur compounds prior to the HCl oxidation process. As mentioned in the Introduction, the guard bed adsorbs the sulfur compounds and simultaneously catalyzes the oxidation CO to CO_2 [20]. However, the catalytic CO oxidation over a noble metal-based catalyst (*e.g.* supported palladium) is expected to suffer from the advancing sulfur poisoning of the guard bed and will require frequent regeneration and even replacement of the catalyst. RuO_2 and IrO_2-based catalysts require the combined removal of CO and sulfur compounds prior to the HCl oxidation step as shown in Scheme 2a. The process can be improved if the removal of CO prior to the HCl

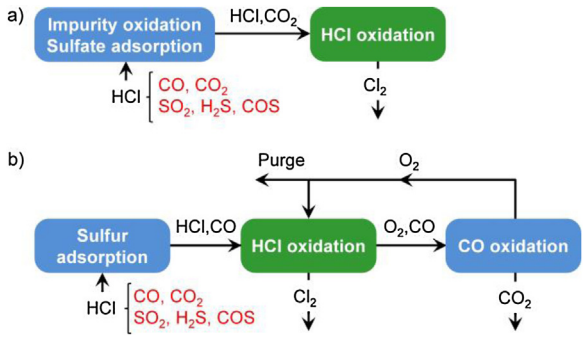

Scheme 2. Chlorine recovery processes with (a) single-step HCl feed purification and (b) a modified process with separated sulfur and CO purification steps. The latter can apply to HCl oxidation catalysts that are insensitive to carbon monoxide, such as CeO_2/ZrO_2.

oxidation step can be omitted. This is possible over CeO_2/ZrO_2, U_3O_8/ZrO_2, and $CuCrO_2$ due to their inactivity for CO oxidation in the presence of HCl. A modified design for the large-scale process over the latter catalysts is proposed in Scheme 2b. The HCl stream from the toluene diisocyanate (TDI) or methylene diphenyl diisocyanate (MDI) synthesis enters the guard bed, where the sulfur compounds are adsorbed. For this step, a cost-effective metal oxide can be used (*e.g.* Al_2O_3, TiO_2, ZrO_2), which is stable against bulk chlorination, adsorbs significant amounts of sulfur compounds at low temperature, and is easy to regenerate [35]. After the HCl oxidation step, the product stream, including the unreacted CO, goes through a multi-step purification process as described elsewhere [10]. To avoid the accumulation of residual CO in the O_2 recycle stream, the CO can be converted to CO_2 by oxidation over a suitable catalyst and removed by gas washing.

5. Conclusions

This study highlights the importance of understanding the impact of feed impurities on the design of an industrial catalytic process for chlorine recycling *via* HCl oxidation. RuO_2/SnO_2-Al_2O_3 and IrO_2/TiO_2 simultaneously oxidized HCl and CO. The high exothermicity of CO oxidation led to a strong bed temperature rise, challenging the safe operation at a large scale. The fixed-bed reactor simulation over the RuO_2-based catalyst underlined the critical occurrence of hot spots and thus the need for a deeply purified HCl stream. In contrast, the oxidation of CO over CeO_2/ZrO_2, U_3O_8/ZrO_2, and $CuCrO_2$ is suppressed under HCl oxidation conditions, thus showing less (no) sensitivity to this impurity. In particular, the ceria-based catalyst yielded a stable chlorine production during 50 h on stream in the presence of CO. The presence of SO_2 and COS severely poisoned all the catalysts due to active site blockage by the sulfur compounds. CeO_2/ZrO_2 deactivated at a lower rate than RuO_2/SnO_2-Al_2O_3, probably due to the higher operating temperature of the former catalyst. The regeneration of sulfur-poisoned catalysts in a diluted feed containing HCl, *i.e.* without O_2, was effective. The RuO_2-based system exhibited a faster and more extended activity recovery than the CeO_2-based system (85% *versus* 50% of the initial activity). This can be tentatively associated with the stronger adsorption of the sulfur on the latter material. On the basis of the above observations, suitable purification strategies have been proposed.

Acknowledgements

We thank Bayer MaterialScience for permission to publish these results. Dr. Timm Schmidt is acknowledged for fruitful discussions and Dr. Markus Hammes for technical assistance with the mass spectrometric analysis.

Appendix A. Supplementary data

Supplementary material related to this article can be found, in the online version, at http://dx.doi.org/10.1016/j.apcatb.2014.07.037.

References

[1] J.G. Firth, H.B. Holland, Nature 212 (1966) 1036–1037.
[2] S.T. Sie, Stud. Surf. Sci. Catal. 6 (1980) 545–569.
[3] T. Shishido, M. Yamamoto, D. Li, Y. Tian, H. Morioka, M. Honda, T. Sano, K. Takehira, Appl. Catal. A 303 (2006) 62–71.
[4] J.P. Boitiaux, J. Cosyns, F. Verna, Stud. Surf. Sci. Catal. 34 (1987) 105–123.
[5] G. Martin, P. Mäki-Arvela, D.Y. Murzin, T. Salmi, Catal. Sci. Technol. 4 (2014) 170–178.
[6] D. Wallenstein, T. Roberie, T. Bruhin, Catal. Today 127 (2007) 54–69.
[7] D. Nicosia, I. Czekaj, O. Kröcher, Appl. Catal. B 77 (2008) 228–236.
[8] Y. Li, J.N. Armor, Appl. Catal. B 1 (1992) L21–L29.
[9] J. Pérez-Ramírez, F. Kapteijn, K. Schöffel, J.A. Moulijn, Appl. Catal. B 44 (2003) 117–151.
[10] J. Pérez-Ramírez, C. Mondelli, T. Schmidt, O.F.-K. Schlüter, A. Wolf, L. Mleczko, T. Dreier, Energy Environ. Sci. 4 (2011) 4786–4799.
[11] C. Mondelli, A.P. Amrute, F. Krumeich, T. Schmidt, J. Pérez-Ramírez, ChemCatChem 3 (2011) 657–660.
[12] M. Moser, C. Mondelli, T. Schmidt, F. Girgsdies, M.E. Schuster, R. Farra, L. Szentmiklósi, D. Teschner, J. Pérez-Ramírez, Appl. Catal. B 132–133 (2013) 123–131.
[13] A.P. Amrute, F. Krumeich, C. Mondelli, J. Pérez-Ramírez, Chem. Sci. 4 (2013) 2209–2217.
[14] M. Moser, C. Mondelli, A.P. Amrute, A. Tazawa, D. Teschner, M.E. Schuster, A. Klein-Hofman, N. López, T. Schmidt, J. Pérez-Ramírez, ACS Catal. 3 (2013) 2813–2822.
[15] A.P. Amrute, G.O. Larrazábal, C. Mondelli, J. Pérez-Ramírez, Angew. Chem. Int. Ed. 52 (2013) 9772–9775.
[16] M. Haas, D. Wastian, T. Loddenkemper, B. Ruffer, US2007/0276158A1, Assigned to Bayer MaterialScience, 2007.
[17] M. Haas, R. Bruns, T. Loddenkemper, EP1992592A2, Assigned to Bayer MaterialScience, 2008.
[18] A. Soppe, K. Werner, US2010/0092373A1, Assigned to Bayer MaterialScience, 2010.
[19] H. Itoh, Y. Kono, M. Ajioka, S. Takenaka, M. Kataita, EP0233773A1, Assigned to Mitsui Toatsu Chemicals, 1987.
[20] M. Haas, M. Dugal, K. Werner, US2010/0266481A1, Assigned to Bayer MaterialScience, 2010.
[21] M. Moser, L. Rodríguez-García, J. Pérez-Ramírez, Ind. Eng. Chem. Res. 53 (2014) 9067–9075.
[22] A. Wolf, L. Mleczko, S. Schubert, O.F.-K. Schlüter, US2007/0274901A1, Assigned to Bayer MaterialScience, 2007.
[23] A.P. Amrute, C. Mondelli, M.A.G. Hevia, J. Pérez-Ramírez, J. Phys. Chem. C 115 (2011) 1056–1063.
[24] Z. Liu, S.J. Jenkins, D.A. King, Phys. Rev. Lett. 93 (2004) 156102.
[25] Y.D. Kim, A.P. Seitsonen, H. Over, Phys. Rev. B 63 (2001) 115419.
[26] J.M.C. Soares, M. Hall, M. Cristofolini, M. Bowker, Catal. Lett. 109 (2006) 103–108.
[27] B. de Rivas, R. López-Fonseca, M.A. Gutiérrez-Ortiz, J.I. Gutiérrez-Ortiz, Appl. Catal. B 104 (2011) 373–381.
[28] D. Teschner, R. Farra, L. Yao, R. Schlögl, H. Soerijanto, R. Schomaecker, T. Schmidt, L. Szentmiklósi, A.P. Amrute, C. Mondelli, J. Pérez-Ramírez, G. Novell-Leruth, N. López, J. Catal. 285 (2012) 273–284.
[29] H. Over, O. Balmes, E. Lundgren, Catal. Today 145 (2009) 236–242.
[30] P.J. Berlowitz, C.H.F. Peden, D.W. Goodman, J. Phys. Chem. 92 (1988) 5213–5221.
[31] T. Luo, R.J. Gorte, Appl. Catal. B 53 (2004) 77–85.
[32] T. Schmidt, T. Loddenkemper, F. Gerhartz, W. Müller, WO2009118095A2, Assigned to Bayer MaterialScience, 2009.
[33] B. Azambre, L. Zenboury, J.V. Weber, P. Burg, Appl. Surf. Sci. 256 (2010) 4570–4581.
[34] P.E. Hoggan, A. Aboulayt, P. Nortier, J.C. Lavalley, J. Catal. 149 (1994) 300–306.
[35] M. Ziolek, J. Kujawa, O. Saur, A. Aboulayt, J.C. Lavalley, J. Mol. Catal. A: Chem. 112 (1996) 125–132.